THE JOURNAL OF PHYSICAL CHEMISTRY C

Article

pubs.acs.org/JPCC

Impact of Surface Ionization on Water Transport and Salt Leakage through Graphene Oxide Membranes

Chao Fang, Zhou Yu, and Rui Qiao*

Department of Mechanical Engineering, Virginia Tech, Blacksburg, Virginia 24061, United States

Supporting Information

ABSTRACT: Nanopores in graphene-based membranes have shown great potential in enabling highly efficient water desalination. The effective engineering of these membranes necessitates a fundamental understanding of how the physical structure and chemical details of their nanopores govern their desalination performance. Using molecular dynamics simulations, we investigate how the ionization of the functional groups along the perimeter of the nanopores in single-layer graphene oxide membranes affects water transport and salt leakage. Moderate ionization enhances water transport and leads to higher salt leakage. With further ionization of the functionalization groups, water flux through the pore is reduced while the salt leakage shows little change. The significant role of functionalization groups' ionization in modulating the water flux and salt leakage through the nanopores is attributed to the different organizations of water molecules and ions in and near the pore as the pore becomes charged due to ionization.

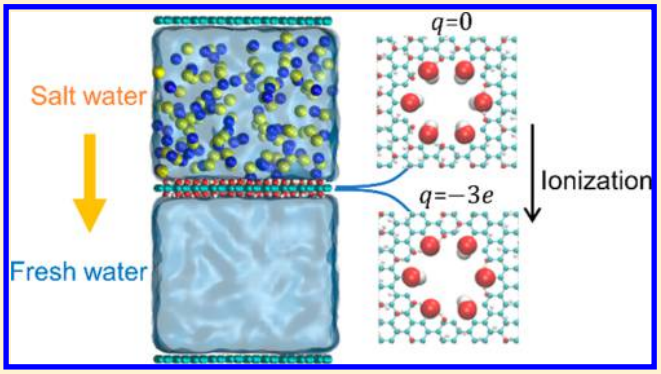

1. INTRODUCTION

The scarcity of fresh water for agricultural, industrial, and human use is a great and growing challenge faced by the society.[1,2] Given the abundance of salt water in seas and aquifers, this challenge can be addressed by purifying salt water using economical processes. Enabled by continuous technological improvements, desalinating salt water to produce fresh water has achieved significant success in recent decades.[3,4] In particular, membrane desalination through reverse osmosis (RO) has advanced significantly and now accounts for over 50% of the installed desalination capacity worldwide.[3] However, RO is still a rather energy intensive process, and there remains a great need to develop membranes with high flux and superior selectivity.[2] A new generation of nanoporous materials can potentially exceed the performance of the classical RO membranes.[5−9] For example, by engineering the pores in these materials with size comparable to water molecules, water flux can be enhanced while maintaining excellent salt rejection.

Recently, single-layer graphene-based membranes showed great potential in desalination due to their atomically thin structure and good chemical stability.[7,10−21] Although the application of these membranes in practical RO operations has yet to materialize, it has been established that the intrinsic/engineered nanopores on graphene's surface provide selective molecular transport.[22] The water and salt transport through these membranes are generally governed by the size and chemistry of the pores in the functionalized or pristine graphene. At a pore diameter of 5.5 Å, permeation of water is allowed and salt ions are effectively rejected.[23] Further increasing the pore size, however, diminishes salt rejection. In addition to their size, the chemistry of the pores, e.g., hydrophobicity, can be leveraged to control the desalination performance of graphene-based membranes.[12,24] For example, nanopores whose edge atoms are terminated by nitrogen and fluorine can act as ionic sieves with high selectivity.[25] Functionalizing the edge of some pores with hydroxyl group can double the water flux through them.[12] While enhancing water flux may not dramatically improve the RO performance due to the thermodynamics limits associated with salt removal, such enhancement is often encouraging because it helps achieve high throughput desalination of water. Other functionalization schemes have also been shown to enable high rejection rate of heavy metal ions and transition-metal ions[26,27] and to more effectively exclude chloride ions.[28]

While previous works provide useful insights into how size and chemistry of the nanopores in graphene-based membranes affect their desalination performance, some issues remain open. Graphene oxide (GO) membranes often contain rich surface functional groups such as the hydroxyl and carboxyl groups. Ionization of these groups can cause the GO membrane to carry net charge. In particular, deprotonation of the carboxyl groups at mild pH leads to buildup of negative charges on the GO layer.[29,30] How ionization of the functionalization groups of GO membrane affects their desalination is not yet clear. On

Received: May 5, 2017
Revised: May 30, 2017
Published: June 1, 2017

DOI: 10.1021/acs.jpcc.7b04283
J. Phys. Chem. C 2017, 121, 13412−13420

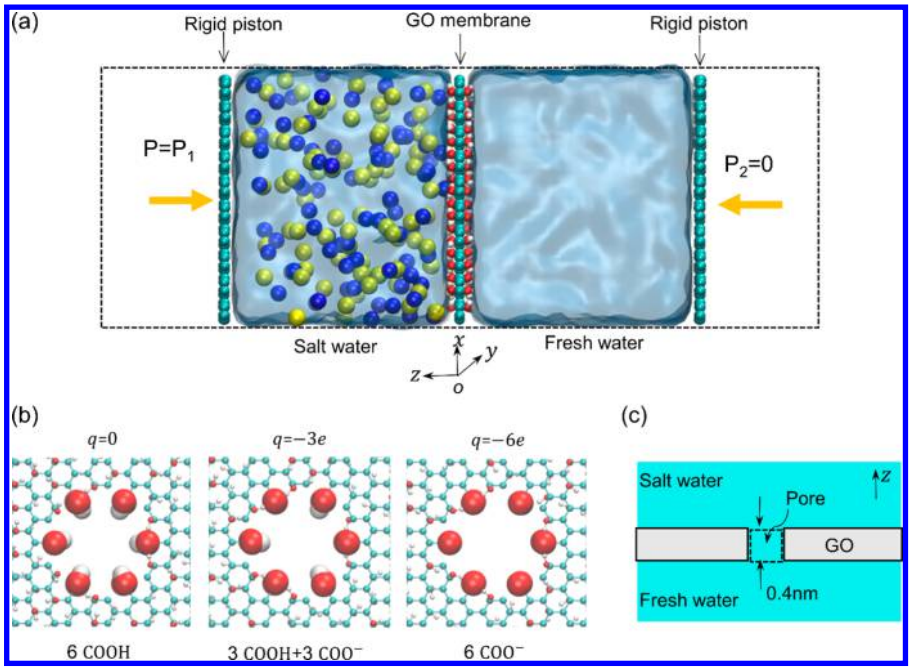

Figure 1. The molecular system used for studying desalination by GO membranes. (a) A side view of the simulation system. The GO membrane has a single nanopore at its center, and six atoms at the perimeter of its pore are functionalized using carboxyl groups. The golden (blue) spheres denote the Na^+ (Cl^-) ions in the salt water. The dashed lines denote the simulation box, which is periodic in all three directions and measures 4.20 × 4.12 nm^2 in the *xy*-plane. (b) Zoom-in views of the nanopores in the GO membrane. The red, cyan, and white spheres denote the oxygen, carbon, and hydrogen atoms, respectively. The carboxyl groups are highlighted as van der Waals spheres. Deprotonation of 0, 3, and 6 of the carboxyl groups results in a net charge of 0, −3*e*, and −6*e* for each pore, respectively. (c) A cutout view of the pore in the GO membrane. A water molecule/ion inside the dashed box (0.4 nm thick) is considered to be within the pore.

the experiment side, previous studies have suggested (though not rigorously proved) that ion selectivity in some graphene membranes was likely due to the negative charge from the ionized functionalization groups.[31] On the theory and simulation side, the effect of ionization of GO membranes' functionalization groups on their desalination has not been examined yet, but useful insight is available from some related studies. In a seminar simulation work, the Striolo group showed that different functionalization groups at the pore edge (hence different distribution of partial charges near the pore) can greatly affect the free energy landscape for ion transport across the pores.[28] Thus, it is safe to assume that the net charge of the nanopores in GO membrane can affect their water and ion transport characteristics and, consequently, the desalination performance of the membrane.

In this work, we aim to investigate how ionization of the functionalization groups at the edge of nanopores in GO membranes affects the desalination behavior of these pores. The rest of the article is organized as follows. We explain the simulation system and methods in section 2. We then present the simulation results on the effects of deprotonation of the carboxyl groups of the nanopores on the water flux and salt leakage through the pores and clarify the molecular physics behind these effects in section 3. Finally, conclusions are drawn in section 4.

2. SIMULATION DETAILS

Figure 1a shows the setup of the simulation system. The system consists of a slab of NaCl solution (salt water) and a slab of fresh water separated by a single-layer GO membrane located at $z = 0$. Two rigid pistons are used to control the pressure of the salt water and fresh water. The system is periodic in all three directions, and the box length in the transmembrane direction (z direction) is 12 nm. Initially, both the salt and fresh water slabs have a thickness of 4 nm, and the salt water has an ion concentration of 2 M. This high salinity helps us obtain good statistics for ion transport through the membrane. We also perform simulations using 1 M salt water and find that the general trend of water and salt transport does not change (see Figures S1 and S2). We note the high salinity of the salt water adopted here is relevant to some practical applications, e.g., the desalination of fluids returned from gas wells to ground after hydraulic fracturing operations.[32]

The GO layer contains hydroxyl groups on its entire surface, and the overall O/C ratio is ∼35%. One nanopore is created at the center of the GO layer by removing selected carbon atoms. Six carboxyl groups are then uniformly functionalized on the edge of the pore. To model ionized carboxyl groups, the hydrogen atoms of the groups are removed. These treatments are consistent with the fact that GO layers contain mostly hydroxyl groups and carboxyl groups.[33,34] and the carboxylic groups on GO's edge are more easily deprotonated under typical pHs.[29] Two pores with nominal diameters of 0.68 and 1.12 nm and the same carboxyl group distribution are considered. The nominal pore diameter is determined as the separation between the carbon atoms of the pair of carboxyl groups positioned diagonally on the pore's perimeter. Following the nomenclature for defected graphene used by the Karnik group, which names pores with different sizes by considering the number of graphene rings removed or partially opened when the pores are created,[35] the small (large) pore used here can be named as P-19 (P-49). The number of ionized carboxyl groups varies among 0, 3, and 6, resulting in 0, −3*e*, and −6*e* charges on the pore (see Figure 1b). When the

DOI: 10.1021/acs.jpcc.7b04283
J. Phys. Chem. C 2017, 121, 13412−13420

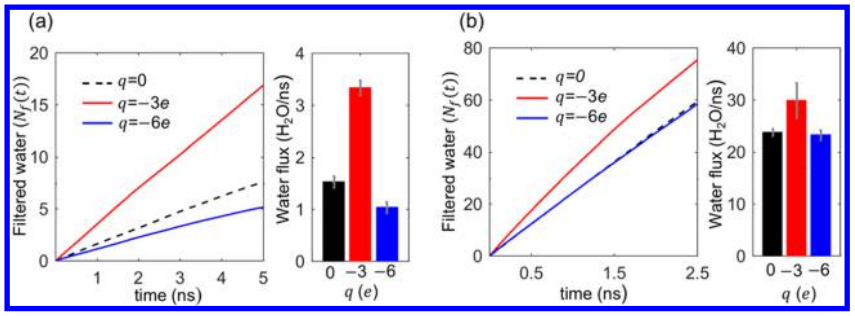

Figure 2. The accumulative number of water molecules filtered through nanopores with different size and charge and the corresponding water flux. (a) Small nanopores with a nominal diameter of 0.68 nm. (b) Large nanopore with a nominal diameter of 1.12 nm. A pressure difference of 100 and 50 MPa between the salt and fresh water is used to drive the water transport through the small and large nanopore, respectively.

carboxyl groups were ionized, 3 or 6 cations are added to the salt water side to maintain the electroneutrality of the whole system. The OPLS-AA force fields are used for the GOs.[28,34,36] The rigid SPC/E model is used for the water molecules.[37] Generally, polarizable force fields afford more accurate prediction of the solvation and dynamics of ions. Because of their very high computational cost, nonpolarizable force fields are adopted. This may reduce the accuracy of predicting water/ion transport.[38] However, some recent work suggests that such inaccuracy may not be significant at graphene−water interfaces.[39] The force fields for the Na^+ and Cl^- ions are adopted from ref 28.

MD simulations are performed using the Gromacs package.[40] The LINCS algorithm is used to constrain all bonds.[41] A NVT ensemble with the velocity-rescale thermostat at 300 K is implemented.[42] A global cutoff 1.2 nm is used for computing the Lennard-Jones potential, and the particle mesh Ewald (PME) method[43] is used to calculate the electrostatic interactions. A large vacuum space is placed outside of the two pistons and their periodical images, and the slab-PME method[44] is used to compute the electrostatic interactions so as to effectively model a 2D system that is periodic only in the GO membrane plane (i.e., *xy*-plane). All carbon atoms in the GO membrane are fixed throughout the simulation. Eliminating the flexibility of the pore's atoms may reduce the water flux. Nevertheless, we note that all functionalization groups along the pore's edge, which affect water transport more significantly than the carbon atoms, can still stretch and bend in our simulations. Therefore, the rigidity of the graphene sheet should not greatly affect the computed water flux.

Initially, the system is equilibrated while fixing the water molecules inside the pore (thus, salt water and fresh water sides are separated). Zero pressure is applied on both pistons, whose atoms are only allowed to move in the *z*-direction. After equilibration for 10 ns, 10−25 configurations are generated and nonequilibrium runs of 5−10 ns are performed. During these nonequilibrium runs, all water molecules and ions are allowed to move freely and the pressure on the piston at the salt water side (P_1) is increased to drive water transport through the pores. The pressure on the piston at the fresh water side is fixed at $P_2 = 0$. Each simulation is repeated 10−25 times with independent initial configurations to obtain good statistics for water and ion transport.

To compute the water and ion flux through the pores accurately, we adopt a method similar to that for computing ion transport through single nanopores.[45] Specifically, the number of filtered water molecules or leaked ions is computed using

$$N_f(t) = \langle n(t) - n(0) \rangle \quad (1)$$

where $n(t)$ is the accumulative number of water molecules or ions passing through the pore and $\langle ... \rangle$ denotes the ensemble average.

3. RESULTS AND DISCUSSION

3.1. Water Flux. To drive the water transport through the GO pores, a large pressure P_1 and a zero pressure P_2 are applied on the left and right pistons shown in Figure 1a, respectively. For the small pores (nominal diameter: 0.68 nm), a P_1 of 100 MPa is used; for the large pores (nominal diameter: 1.12 nm), a P_1 of 50 MPa is used. A higher P_1 is used for the small pores because of the larger resistance for water transport in these pores. The high pressure used is necessary to achieve notable water flux within the time scale accessible by MD simulations and is similar to those used in prior simulation studies.[7,12,26] We also conduct simulations with $P_1 = 50$ MPa for the small pores and $P_1 = 20$ MPa for the large pores and find the obtained water and salt transport characteristics are similar to the results presented below (see Figure S3).

Figure 2 shows the water transport behavior of all the pores. We observe that the number of filtered water molecules $N_f(t)$ increases linearly with time and depends on the pore charge. We also compute the water flux through pore by linear regression of $N_f(t)$. For the small pores, as their charge changes from $q = 0$ to $q = -3e$, the water flux more than doubles. However, as their charge changes further to $q = -6e$, the water flux becomes even smaller than that at $q = 0$. Similar effects of pore charge on the water flux are also observed for the large pores, albeit to a lesser extent. These results indicate that ionization of the pores' functional groups affects the water flux through pores: moderate ionization greatly enhances water flux but too strong ionization can diminish the water flux, and the strength of these effects depends strongly on the pore size.

The increase of water flux as the pore charge changes from $q = 0$ to $-3e$ can be attributed to the increased "effective" pore size. To probe the effective size of the pores, we calculate the lateral distribution of water molecules within a 0.4 nm thick slab centered on each pore (see the dashed box in Figure 1c; water molecules within this slab are considered to be inside the pore hereafter). Figure 3 shows the *xy*-plane density map of water inside the small pores, and the carboxyl groups on the pores' edge are also highlighted. The water distribution is similar for pores with different charges; e.g., six high-density sites, which provide a gateway for water transport through the pore, are observed near the carboxyl groups (some are ionized) at the pore edge. As the pore becomes more negatively charged,

DOI: 10.1021/acs.jpcc.7b04283
J. Phys. Chem. C 2017, 121, 13412−13420

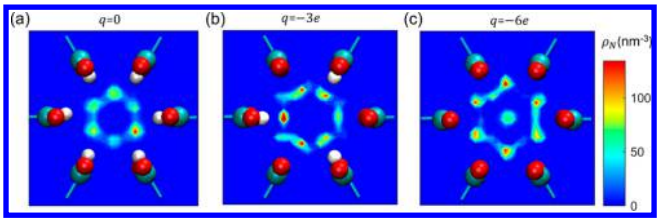

Figure 3. The *xy*-plane distribution of water molecules inside the small pore with a nominal diameter of 0.68 nm. The pore's net charge is q = 0, $-3e$, and $-6e$ in the three panels. The carboxyl groups (neutral and ionized) along the pore's perimeter are shown as van der Waals spheres (hydrogen, oxygen, and carbon atoms are in white, red, and cyan color, respectively).

these sites are drawn closer to the carboxyl groups. In fact, when the pore charge reaches $q = -6e$, an extra high-density site appears at the pore center. Meanwhile, the number of water molecules at these high-density sites increases; e.g., the total number of water molecules inside the pore increases from 5.82 to 6.87 and 8.00 as pore charge changes from 0 to $-3e$ and $-6e$. Clearly, by drawing water molecules closer to the pore edge and accommodating more water molecules in the pore, ionization of the pore's carboxyl groups effectively enlarges the pore. This pore widening effect originates from the stronger electrostatic interactions of water molecules with the COO^- group (dipole−charge interactions) than with the COOH group (dipole−dipole interactions) and helps explain why water flux is higher through the $q = -3e$ pore than through the neutral pore. This enhancement is consistent with the reports that water flux through graphene pores can be enhanced by increasing the water−pore interactions via functionalization of the pores' pristine edge.[46,47] Our results suggest that ionization of the functionalization groups already on the pore's edge can be another strategy for controlling the water−pore interactions and thus the water flux.

The above pore widening effect, however, cannot explain why the water flux decreases below that for neutral pores when the pore charge changes from $q = -3e$ to $-6e$. To understand this unexpected behavior, we analyze the distribution and the energetics of water molecules across the pore through separate equilibrium simulations. Specifically, we perform simulations with the same salt water on both sides of the membrane and zero pressure on both pistons. Figure 4a shows the one-dimensional (1D) water density distribution along the pore axis (see Figure 4a inset). Because the functionalized groups at the pore edge are not exactly symmetrically distributed with respect to the horizontal plane of the pore ($z = 0$), the water density profile is not precisely symmetrical with respect to this plane. Here, to facilitate discussion and to improve statistics, the water density profile through the pores is symmetrized with respect to the pores' horizontal plane. Figure 4a shows that as the pore becomes more negatively charged, the water density within 0.2 nm from the pore's horizontal plane increases, and this is consistent with that observed from the *xy*-plane water density map inside the pores (see Figure 3).

From the distribution of water molecules in Figure 4a, we can extract their 1D potential of mean force (PMF) through the pores using $\mathrm{PMF}(z) = -k_B T \ln \rho(z)/\rho_0$, where T is the temperature, k_B is the Boltzmann constant, and ρ_0 is the water density at position far from the pore where the PMF is taken as zero. While the 1D PMF thus calculated does not fully capture the three-dimensional pathway and free energy landscape for water permeation, it does provide a semiquantitative under-

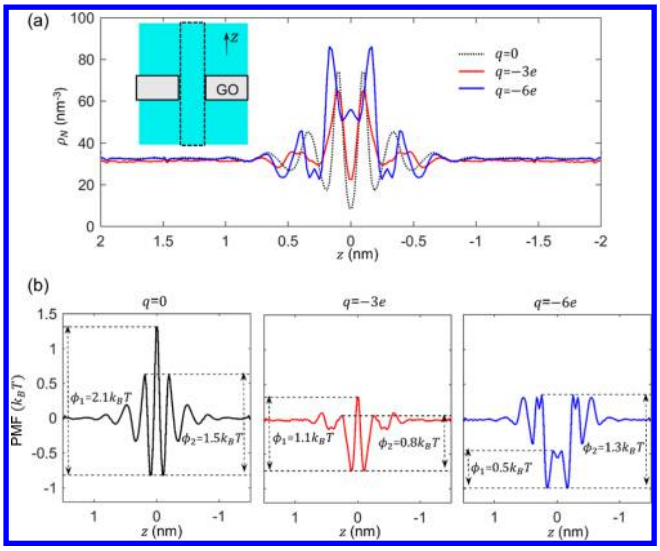

Figure 4. Distribution and energetics of water molecules across nanopores with a nominal diameter of 0.68 nm. (a) The one-dimensional (1D) density profiles of water molecules along the axis of pores with q = 0, $-3e$, and $-6e$. Only water molecules within a radius of 0.34 nm (labeled by the dashed box in the inset) from the pore axis are considered. The GO membrane is located at $z = 0$. (b) The 1D potential of mean force (PMF) profiles of water molecules along the axis of pores with different charges. The major energy barriers for water molecules to translocate the pore (ϕ_1) and to approach the pore from bulk or leave the pore toward bulk (ϕ_2) are labeled by the dashed lines.

standing of the energetics for water transport through the pore. As shown in Figure 4b, for a water molecule to migrate from the bulk water from one side of the membrane to that at the other side, it must overcome three key energy barriers regardless of the charge on the pore: one barrier with a height of ϕ_1 as it crosses the pore's horizontal plane and two barriers with a height of ϕ_2 as it reaches the pore from the bulk water (or vice versa). As the pore charge changes from 0 to $-3e$, the energy barrier ϕ_1 is reduced from $2.1k_BT$ to $1.1k_BT$ and ϕ_2 is reduced from $1.5k_BT$ to $0.8k_BT$. Therefore, water molecules translocating the $q = -3e$ pore has to overcome smaller energy barriers comparing to that for the $q = 0$ pore. Thus, the enhanced water flux at $q = -3e$ pore than the neutral pore is also expected from the energetics of water transport across the pore.

As the pore charge changes from $-3e$ to $-6e$, the height of the energy barrier ϕ_1 decreases from $1.1k_BT$ to $0.5k_BT$; the height of the energy barrier ϕ_2, however, increases from $0.8k_BT$ to $1.3k_BT$. In addition, further away from the membrane, the PMF is more corrugated for the pore with $q = -6e$ when compared with the pore with $q = -3e$. Therefore, the transport of water molecules through the pore with $q = -6e$ is energetically less favorable than that through the pore with $q = -3e$, thus helping explain the decrease of water flux as pore charge changes from $q = -3e$ to $-6e$. However, the energy barriers for water transport through the pore with $q = -6e$ are smaller than through the pore with $q = 0$. This suggests that the small water flux through the pore with $q = -6e$ pore cannot be explained based on the energetics of water transport alone. Here we postulate that the dynamics of water in the pore is slowed down as the pore charge increases and the water flux through the pore with $q = -6e$ is smaller than other pores

DOI: 10.1021/acs.jpcc.7b04283
J. Phys. Chem. C 2017, 121, 13412−13420

because the dynamics of water is slowed down the most in this pore.

Directly quantifying the dynamics of water inside the GO pores is difficult because the pore is thin and there exists significant local gradient of PMF through the pore. Here we use an indirect method for inferring the dynamics of water molecules inside pores from equilibrium simulations with the same salt water on both sides of the membrane and zero pressure on both pistons. We define an occupancy autocorrelation function for water molecules inside the pore

$$C_R(t) = \langle P_R(t)P_R(0)\rangle / \langle P_R(0)^2\rangle \quad (2)$$

where $P_R(t)$ is a binary function that is equal to 1 if a water molecule in the pore at time 0 is also found at time t and is equal to 0 otherwise. $\langle ...\rangle$ denotes the ensemble average. From the decay of $C_R(t)$ with time, we can infer the residence time of water molecules in the pore and thus their dynamics indirectly. Figure 5a shows the $C_R(t)$ computed for water molecules inside small pores with different charges. For pores with $q = 0$, $C_R(t)$ decays to 0.1 at $t = 1.56$ ns, suggesting that water molecules inside the pore readily leave the pore and thus are highly mobile. In pores with $q = -3e$, $C_R(t)$ decays slightly slower and reaches 0.1 at $t = 1.01$ ns. However, in pores with $q = -6e$, $C_R(t)$ decays much more slowly and is 0.24 at $t = 4$ ns, indicating that once a water molecule enters this pore, it stays inside much longer than in pores with $q = 0$ and $-6e$. The much longer residence time in pores with $q = -6e$ is not mainly caused by higher energy barriers for water inside the pore to leave the pore but by the slower dynamics of water inside the highly charged pores. As shown in Figure 4b, water escaping a pore must overcome an energy barrier ϕ_2 and ϕ_2 is close for pores with $q = 0$ ($\phi_2 = 1.5k_BT$) and pores with $q = -6e$ ($\phi_2 = 1.3k_BT$). Since the escape rate of a water molecules from a pore is controlled primarily by the energy landscape for its escape and its mobility, the latter result suggests that the much longer residence time of water molecules inside pores with $q = -6e$ than with $q = 0$ is caused by the slower dynamics of water molecules inside the highly charged pore. Such slower dynamic of the water molecules in the highly charged pores helps explain why the water flux through pores with $q = -6e$ is smaller than that through pores with $q = 0$ even though the energy barriers for water translocation are higher for pores with $q = 0$.

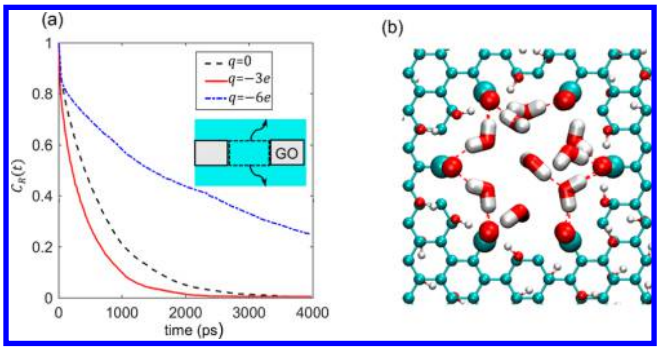

Figure 5. Structure and dynamics of water molecules inside pores. (a) The occupancy autocorrelation function of water molecules in pores with a nominal diameter of 0.68 nm and different charges. A water molecule occupies the pore if it is within the dashed box labeled in the inset. (b) A snapshot of the water molecules in the small pore (nominal diameter: 0.68 nm) with $q = -6e$. The COO^- groups are shown as van der Waals spheres, with color coding same as that in Figure 1. The red dashed lines denote the hydrogen bonds formed between water molecules and between water molecules and the COO^- groups. Geometrical criteria ($d_{O-O} \leq 0.35$ nm and $\angle HOH \leq 30°$) are used for hydrogen bonding analysis.[48]

The slower dynamics of water molecules inside pores with $q = -6e$ than pores with $q = 0$ and $-3e$ is closely related to their molecular organization inside the highly charged pores. As a pore becomes more negatively charged, the number of water molecules inside it increases and these water molecules approach the carboxyl groups on the pore's edge more closely (see Figure 3). Inside the pore, water molecules form more ordered structure in the $q = -6e$ pore than in the $q = 0$ and $q = -3e$ pores as evident from the angle distribution of dipole moment of the water molecules inside the pore (see Figure S4). In addition, in pores with $q = -6e$, water molecules form strong hydrogen bonds with the COO^- groups (some water molecules can even form hydrogen bonds with two COO^- groups simultaneously, see Figure 5b), which results in highly stabilized water structure in the pore and consequently slow water dynamics.

In the above calculations, the salt concentration in the feeding solution (2 M) is much higher than common salt water such as seawater. The higher salt concentration leads to a higher osmotic pressure, and thus it requires higher pressure to drive the RO process. In addition, the elevated ion concentration in the feeding solution can also affect water flux through other mechanisms. For example, in our simulations of water transport through the 1.12 nm wide pores at a pressure difference of 50 MPa, when the salt concentration in the feeding solution increases from 1 to 2 M, the driving force for RO decreases ~10% due to the increased osmotic pressure.

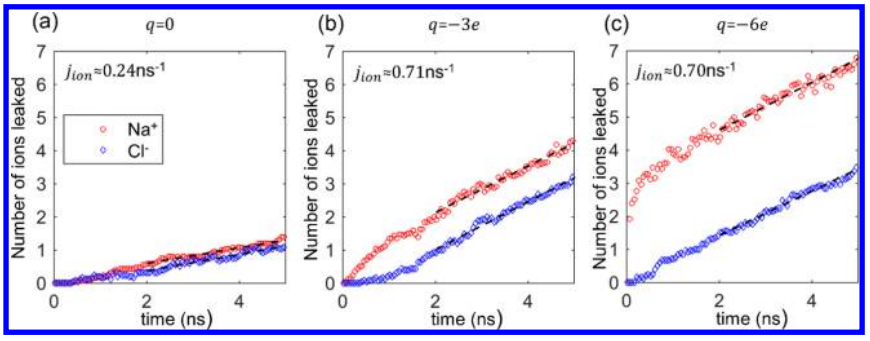

Figure 6. Evolution of the number of ions leaked through large pores (nominal diameter: 1.12 nm) with net charge $q = 0$, $-3e$, and $-6e$. The dashed lines denote linear regression at time larger than 2 ns. A pressure difference of 50 MPa between the salt and fresh water sides is used to drive the water transport.

DOI: 10.1021/acs.jpcc.7b04283
J. Phys. Chem. C 2017, 121, 13412−13420

Our simulations, however, showed that the water flux decreases by 33 ± 3%, 21 ± 7%, and 16 ± 6% for pores with charge of q = 0, $-3e$, and $-6e$, respectively. The more significant decrease of water flux revealed in our simulations is likely caused by the slower dynamics of water molecules in solutions with higher salt concentrations.

3.2. Salt Leakage. The leakage of salt ions through GO pores is another important aspect of their desalination performance. While pores must exceed certain critical diameter to allow water transport, they must also be narrow enough to hinder the leakage of salt ions. For the small pores with a nominal diameter of 0.68 nm, no salt leakage is observed with the pressures applied here during our MD simulations. For large pores with a nominal diameter of 1.12 nm, leakage of Na^+ and Cl^- ions is observed during our simulation. Because large pores inevitably exist in practical GO membranes, it is useful to study how salt leaks through these pores in detail.

Figure 6 shows the accumulative leakage of Na^+ and Cl^- ions through the 1.12 nm wide pore with different charges when $P_1 - P_2$ = 50 MPa. When the pore is neutral, the leakage of Na^+ and Cl^- ions is indistinguishable within statistical uncertainty. When the pore is negatively charged, initially, the Cl^- (Na^+) ions leak through the pore slower (faster) because the Cl^- (Na^+) ions are repelled from (attracted to) the negatively charged pores. However, at large time, the leakage rate of Na^+ and Cl^- ions becomes the same, and the difference between the number of Na^+ and Cl^- ions leaked through the pore stabilizes at ∼1.5e and ∼3e for the pore with $q = -3e$ and $-6e$, respectively. The former is simply a consequence of the fact that the net electrical current is zero in the present system. The latter is consistent with the observation that the pore charge is equally balanced by ions at the GO membrane's two sides (see Figure S5). Using the linear regression of the ion leakage data in Figure 6, the salt leakage rate j_{ion} (i.e., the pairs of Na^+/Cl^- ions leaked through the pore per unit time) is determined as j_{ion} = 0.24, 0.71, and 0.70 ns^{-1} for pores with q = 0, $-3e$, and $-6e$, respectively. Thus, j_{ion} increases sharply as the pore's charge changes from 0 to $-3e$ but changes little as the pore charge changes further to $-6e$.

The evolution of j_{ion} in pores with their charges is closely correlated with the evolution of ion occupancy in these pores. Because ions in a pore provide gateways for ion transport through the pore, higher occupancy of ions inside the pore facilitates the ion leakage through it. Table 1 shows the number of Na^+ and Cl^- ions inside the pores studied in Figure 6 (similar to water molecules, ions within 0.2 nm from the pore's horizontal plane are taken as inside the pore; see the dashed box in Figure 1c). Because the leakage of a cation through any pore must be balanced by the leakage of an anion and vice versa, j_{ion} is controlled primarily by the leakage of the minority ions inside the pore. In neutral pores, Na^+ ions are the minority ion. When confined inside a neutral pore, an ion tends to lose part of its hydration water molecules because the density of water inside the pore is low. We found that a Na^+ ion inside the neutral pore loses ∼25% of its hydration water molecules compared to ∼10% for the Cl^- ion. Therefore, it is energetically less favorable to insert a Na^+ ion into the neutral pore than the Cl^- ions and Na^+ ions are the minority ion inside the pore. In this case, ion exclusion due to the dehydration barrier caused by small pore size plays a key role in determining the ion occupancy in the pore (and consequently the salt leakage through the pore).[49] In charged pores, Cl^- ions are the minority ion since they are repelled from the pores by the negative pore charge. Here, co-ion exclusion due to the electrostatic repulsion by the charged functional groups plays a key role in determining the ion occupancy in the pore.[49] Table 1 shows that the occupancy of the minority Cl^- ions in pores with $q = -3e$ is much higher than the occupancy of the minority Na^+ ions in the neutral pores, which leads to the higher j_{ion} in the pores with $q = -3e$. When the pore is more negatively charged, the occupancy of the minority Cl^- ions increases marginally, and thus j_{ion} is comparable with that through pores with $q = -3e$. These observations are initially unexpected. According to the mean-field theories for electrical double layers, the co-ion concentration within a few Debye lengths from a highly charged object is much lower than that in bulk electrolytes and *decreases* as the charge on the object increases.[50] For electrolytes with monovalent ions, their Debye length is given by $\lambda_D = \sqrt{\epsilon k_B T/2e^2 c_\infty}$, where ϵ and c_∞ are the their dielectric permittivity and bulk concentration, respectively. Here, the salt water at the GO membrane's feed side has a concentration of 2 M, hence a Debye length of 0.2 nm. Because the pore carries a large charge density (∼−0.8e/nm per unit length of the perimeter for the pores with $q = -3e$), Cl^- ions are largely repelled from the pore (water accessible radius: ∼0.5 nm) and the occupancy of Cl^- ions inside the pore should decrease as the pore charge changes from $-3e$ to $-6e$, in contrast to the marginal increase shown in Table 1.

To understand the high Cl^- ion occupancy in pores with $q = -6e$, we examine the distribution of Na^+ and Cl^- ions in and around the pores in detail. Figure 7a shows the ion density distribution as a function of radial and axial distance from the pore center. As expected, a significant amount of Na^+ ions is accumulated near the pore's perimeter to screen COO^- groups' charge. However, many Cl^- ions accumulate in the central portion of the pore, despite the electrostatic repulsion by the COO^- groups (similar distribution is observed for pores with $q = -3e$, see Figure S6). The accumulation of Cl^- ions in the pore's center is attributed to the strong correlations between

Table 1. Occupancy of Salt Ions in the Large Pore (Nominal Diameter: 1.12 nm) with Different Charges[a]

pore charge q	0	$-3e$	$-6e$
Na^+ ion	0.11	0.95	3.49
Cl^- ion	0.79	0.50	0.61

[a]An ion is considered to occupy the pore if it is within the dashed box shown in Figure 1c.

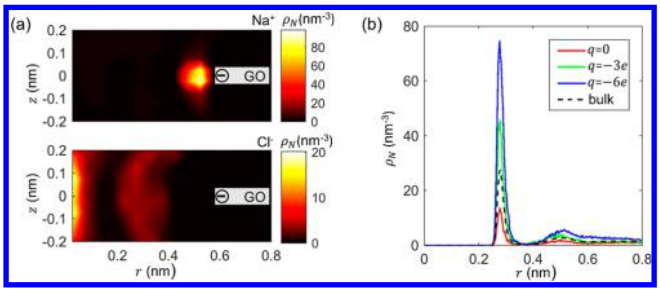

Figure 7. (a) Distribution of Na^+ ions (upper panel) and Cl^- ions (lower panel) inside and near a large pore with $q = -6e$. z = 0 and r = 0 denote the pore's horizontal plane and vertical axis, respectively. (b) Radial density distribution of Cl^- ions around the Na^+ ions inside the large pore with different charge q and in bulk 2 M NaCl solution.

DOI: 10.1021/acs.jpcc.7b04283
J. Phys. Chem. C 2017, 121, 13412−13420

Na^+ and Cl^- ions, which are neglected in the mean-field theories for electrical double layers. To show this, we computed the distribution of Na^+ ions around the Cl^- ions inside the pore (see Figure 7b). Figure 7b shows that Cl^- ions are "coordinated" by Na^+ ions both in bulk electrolytes and inside the pore. The coordination of Cl^- ions by Na^+ ions is enhanced when the pore becomes more negatively charged, mostly because more Na^+ ions are brought near the pore when the pore's charge changes from $-3e$ to $-6e$. Such an improved coordination compensates the enhanced repulsion by the COO^- groups, and thus the occupancy of Cl^- ions inside the pore changes little.

In the above discussion, the salt concentration in the feed solution is 2 M, which is much higher than that in seawater and brackish water. The elevated salt concentration used in our simulations leads to weaker electrostatic repulsion of co-ion from pore (due to enhanced screening of electrostatic interactions by ions) and stronger ion−ion correlations than those in seawater. Since weaker electrostatic repulsion and weaker ion−ion correlations both tend to increase the occupancy of co-ions in charged pores, we expect the leakage of ions through the pore exposed to seawater to be less severe than that predicted in our simulations. Nevertheless, the effect of pore charge on the salt leakage should not change qualitatively for seawater because seawater itself is highly concentrated (its Debye length is only 22% and 45% smaller than that of the 1 and 2 M salt water used here). For brackish water with low ion concentration (say ∼0.1 M), the conclusions obtained here may need to be reassessed through systematic studies.

So far, we have focused on the absolute rate of salt leakage. In practice, the salt rejection rate is considered an important metric in evaluating the performance of reverse osmosis membranes. We thus calculate the salt rejection rate using the salt leakage rate and the corresponding water flux obtained above. For the small pores, the salt rejection rate is 100%. For the large pore with a nominal diameter of 1.12 nm, when the desalination is driven by a pressure difference of 50 MPa, the salt rejection rates are 76%, 42%, and 22% for pore charges of 0, $-3e$, and $-6e$, respectively. Therefore, ionizing the carboxyl groups of the large pores considered here compromises their salt rejection rate, especially if the level of ionization is high. Since modest ionization of the carboxyl groups actually increases the water flux, this result suggests that one should consider the trade-off between the water flux and salt rejection rate when assessing the effect of ionization on the performance of GO membranes.

4. CONCLUSIONS

In summary, we investigate how the nanopore structure and chemistry affect the desalination behavior of single-layer GO membranes. We show that ionizing the functionalization groups on nanopores' perimeter affects both the water flux and salt leakage through the nanopore and the effect depends on the degree of ionization and the size of the pore. Modest ionization lowers the energy barrier for water translocation through the pores and thus enhances the water flux. Severe ionization, however, reduces the water flux because the dynamics of water molecules inside the pores is slowed down by the strong interactions between ionized functionalization groups and water molecules. These effects are pronounced for pores with a nominal diameter of 0.68 nm but weak for pores with a nominal diameter of 1.12 nm. Generally, ionization enhances salt leakage through the pores comparing to neutral pores by increasing the occupancy of ions inside the pore. As the degree of ionization increases, the occupancy of the co-ions does not decrease as expected from classical mean-field theories but increase slightly; thus, salt leakage does not change greatly for the pores studied here. The unexpected increase of co-ion occupancy inside the pores with the increasing pore charge is attributed to the strong correlations between counterions and co-ions.

GO membranes carry numerous functionalization groups and can become charged due to the ionization of these functionalization groups. The ionization of these groups is controlled by the operation conditions of the membrane, most importantly the pH of its feed solution. Our study thus suggests that the operation conditions (especially the pH) can have a significant effect on the membrane's desalination performance, and attention should be paid to such conditions when designing/selecting membranes for a target desalination application. This necessarily complicates membrane design/selection; e.g., the finding that increasing ionization of the functionalization group leads to decreased salt rejection rate but nonmonotonic variation of water flux suggests that the trade-off between water flux and salt rejection rate must be considered. However, this finding also suggests that ionization of the functionalization groups can potentially be leveraged to develop better GO membranes. In particular, although enhancing water flux may not dramatically improve the performance of these membranes due to the thermodynamics limits associated with salt removal, increased water flux can be very useful when high throughput is needed in desalination operations.

■ ASSOCIATED CONTENT

Supporting Information

The Supporting Information is available free of charge on the ACS Publications website at DOI: 10.1021/acs.jpcc.7b04283.

Water and salt transport characteristics under different salt water concentrations and pressure differences between salt and fresh water sides, angle distribution of water dipole inside the large pore, balance of pore charge by ions in the system, and ion distribution near large pores with $q = -3e$ (PDF)

■ AUTHOR INFORMATION

Corresponding Author

*E-mail: ruiqiao@vt.edu.

ORCID

Rui Qiao: 0000-0001-5219-5530

Notes

The authors declare no competing financial interest.

■ ACKNOWLEDGMENTS

We thank the support from the Institute for Critical Technology and Applied Science (ICTAS) at Virginia Tech. We also thank the ARC for generous allocations of computer time on the BlueRidge and NewRiver clusters.

■ REFERENCES

(1) Elimelech, M.; Phillip, W. A. The Future of Seawater Desalination: Energy, Technology, and the Environment. *Science* **2011**, *333*, 712−717.

DOI: 10.1021/acs.jpcc.7b04283
J. Phys. Chem. C 2017, 121, 13412−13420

(2) Shannon, M. A.; Bohn, P. W.; Elimelech, M.; Georgiadis, J. G.; Marinas, B. J.; Mayes, A. M. Science and Technology for Water Purification in the Coming Decades. *Nature* **2008**, *452*, 301−310.
(3) Zhou, Y.; Tol, R. S. J. Evaluating the Costs of Desalination and Water Transport. *Water Resour. Res.* **2005**, *41*, W03003.
(4) Veerapaneni, S. V.; Long, B.; Freeman, S.; Bond, R. Reducing Energy Consumption for Seawater Desalination. *J. Am. Water Works Assoc.* **2007**, *99*, 95.
(5) Fornasiero, F.; Park, H. G.; Holt, J. K.; Stadermann, M.; Grigoropoulos, C. P.; Noy, A.; Bakajin, O. Ion Exclusion by Sub-2-Nm Carbon Nanotube Pores. *Proc. Natl. Acad. Sci. U. S. A.* **2008**, *105*, 17250−17255.
(6) Zhao, Y.; Xie, Y.; Liu, Z.; Wang, X.; Chai, Y.; Yan, F. Two-Dimensional Material Membranes: An Emerging Platform for Controllable Mass Transport Applications. *Small* **2014**, *10*, 4521−4542.
(7) Suk, M. E.; Aluru, N. Water Transport through Ultrathin Graphene. *J. Phys. Chem. Lett.* **2010**, *1*, 1590−1594.
(8) Heiranian, M.; Farimani, A. B.; Aluru, N. R. Water Desalination with a Single-Layer Mos2 Nanopore. *Nat. Commun.* **2015**, *6*, 8616.
(9) Humplik, T.; Lee, J.; O'hern, S.; Fellman, B.; Baig, M.; Hassan, S.; Atieh, M.; Rahman, F.; Laoui, T.; Karnik, R. Nanostructured Materials for Water Desalination. *Nanotechnology* **2011**, *22*, 292001.
(10) Surwade, S. P.; Smirnov, S. N.; Vlassiouk, I. V.; Unocic, R. R.; Veith, G. M.; Dai, S.; Mahurin, S. M. Water Desalination Using Nanoporous Single-Layer Graphene. *Nat. Nanotechnol.* **2015**, *10*, 459−464.
(11) Celebi, K.; Buchheim, J.; Wyss, R. M.; Droudian, A.; Gasser, P.; Shorubalko, I.; Kye, J.-I.; Lee, C.; Park, H. G. Ultimate Permeation across Atomically Thin Porous Graphene. *Science* **2014**, *344*, 289−292.
(12) Cohen-Tanugi, D.; Grossman, J. C. Water Desalination across Nanoporous Graphene. *Nano Lett.* **2012**, *12*, 3602−3608.
(13) Han, Y.; Xu, Z.; Gao, C. Ultrathin Graphene Nanofiltration Membrane for Water Purification. *Adv. Funct. Mater.* **2013**, *23*, 3693−3700.
(14) Rollings, R. C.; Kuan, A. T.; Golovchenko, J. A. Ion Selectivity of Graphene Nanopores. *Nat. Commun.* **2016**, *7*, 11408.
(15) Wang, Y.; He, Z.; Gupta, K. M.; Shi, Q.; Lu, R. Molecular Dynamics Study on Water Desalination through Functionalized Nanoporous Graphene. *Carbon* **2017**, *116*, 120−127.
(16) Qiu, Y.-H.; Li, K.; Chen, W.-Y.; Si, W.; Tan, Q.-Y.; Chen, Y.-F. Ion and Water Transport in Charge-Modified Graphene Nanopores. *Chin. Phys. B* **2015**, *24*, 108201.
(17) Geim, A. K.; Novoselov, K. S. The Rise of Graphene. *Nat. Mater.* **2007**, *6*, 183−191.
(18) Geim, A. K. Graphene: Status and Prospects. *Science* **2009**, *324*, 1530−1534.
(19) Dreyer, D. R.; Park, S.; Bielawski, C. W.; Ruoff, R. S. The Chemistry of Graphene Oxide. *Chem. Soc. Rev.* **2010**, *39*, 228−240.
(20) Huang, H. B.; Ying, Y. L.; Peng, X. S. Graphene Oxide Nanosheet: An Emerging Star Material for Novel Separation Membranes. *J. Mater. Chem. A* **2014**, *2*, 13772−13782.
(21) Huang, H.; Ying, Y.; Peng, X. Graphene Oxide Nanosheet: An Emerging Star Material for Novel Separation Membranes. *J. Mater. Chem. A* **2014**, *2*, 13772−13782.
(22) O'Hern, S. C.; Stewart, C. A.; Boutilier, M. S.; Idrobo, J.-C.; Bhaviripudi, S.; Das, S. K.; Kong, J.; Laoui, T.; Atieh, M.; Karnik, R. Selective Molecular Transport through Intrinsic Defects in a Single Layer of Cvd Graphene. *ACS Nano* **2012**, *6*, 10130−10138.
(23) Iwasaki, T.; Park, H. J.; Konuma, M.; Lee, D. S.; Smet, J. H.; Starke, U. Long-Range Ordered Single-Crystal Graphene on High-Quality Heteroepitaxial Ni Thin Films Grown on Mgo (111). *Nano Lett.* **2011**, *11*, 79−84.
(24) Alexiadis, A.; Kassinos, S. Molecular Simulation of Water in Carbon Nanotubes. *Chem. Rev.* **2008**, *108*, 5014−5034.
(25) Sint, K.; Wang, B.; Král, P. Selective Ion Passage through Functionalized Graphene Nanopores. *J. Am. Chem. Soc.* **2008**, *130*, 16448−16449.
(26) Kommu, A.; Namsani, S.; Singh, J. K. Removal of Heavy Metal Ions Using Functionalized Graphene Membranes: A Molecular Dynamics Study. *RSC Adv.* **2016**, *6*, 63190−63199.
(27) Sun, P. Z.; Liu, H.; Wang, K. L.; Zhong, M. L.; Wu, D. H.; Zhu, H. W. Selective Ion Transport through Functionalized Graphene Membranes Based on Delicate Ion-Graphene Interactions. *J. Phys. Chem. C* **2014**, *118*, 19396−19401.
(28) Konatham, D.; Yu, J.; Ho, T. A.; Striolo, A. Simulation Insights for Graphene-Based Water Desalination Membranes. *Langmuir* **2013**, *29*, 11884−11897.
(29) Konkena, B.; Vasudevan, S. Understanding Aqueous Dispersibility of Graphene Oxide and Reduced Graphene Oxide through Pka Measurements. *J. Phys. Chem. Lett.* **2012**, *3*, 867−872.
(30) Shih, C.-J.; Lin, S.; Sharma, R.; Strano, M. S.; Blankschtein, D. Understanding the Ph-Dependent Behavior of Graphene Oxide Aqueous Solutions: A Comparative Experimental and Molecular Dynamics Simulation Study. *Langmuir* **2012**, *28*, 235−241.
(31) O'Hern, S. C.; Boutilier, M. S. H.; Idrobo, J.-C.; Song, Y.; Kong, J.; Laoui, T.; Atieh, M.; Karnik, R. Selective Ionic Transport through Tunable Subnanometer Pores in Single-Layer Graphene Membranes. *Nano Lett.* **2014**, *14*, 1234−1241.
(32) Fakcharoenphol, P.; Kurtoglu, B.; Kazemi, H.; Charoenwongsa, S.; Wu, Y.-S. In *The Effect of Osmotic Pressure on Improve Oil Recovery from Fractured Shale Formations*; SPE unconventional resources conference; Society of Petroleum Engineers: 2014.
(33) Wei, N.; Peng, X.; Xu, Z. Understanding Water Permeation in Graphene Oxide Membranes. *ACS Appl. Mater. Interfaces* **2014**, *6*, 5877−5883.
(34) Tang, H.; Liu, D.; Zhao, Y.; Yang, X.; Lu, J.; Cui, F. Molecular Dynamics Study of the Aggregation Process of Graphene Oxide in Water. *J. Phys. Chem. C* **2015**, *119*, 26712−26718.
(35) Sun, C.; Boutilier, M. S.; Au, H.; Poesio, P.; Bai, B.; Karnik, R.; Hadjiconstantinou, N. G. Mechanisms of Molecular Permeation through Nanoporous Graphene Membranes. *Langmuir* **2014**, *30*, 675−682.
(36) Jorgensen, W. L.; Maxwell, D. S.; Tirado-Rives, J. Development and Testing of the Opls All-Atom Force Field on Conformational Energetics and Properties of Organic Liquids. *J. Am. Chem. Soc.* **1996**, *118*, 11225−11236.
(37) Berendsen, H.; Grigera, J.; Straatsma, T. The Missing Term in Effective Pair Potentials. *J. Phys. Chem.* **1987**, *91*, 6269−6271.
(38) Striolo, A.; Michaelides, A.; Joly, L. The Carbon-Water Interface: Modeling Challenges and Opportunities for the Water-Energy Nexus. *Annu. Rev. Chem. Biomol. Eng.* **2016**, *7*, 533−556.
(39) Ho, T. A.; Striolo, A. Polarizability Effects in Molecular Dynamics Simulations of the Graphene-Water Interface. *J. Chem. Phys.* **2013**, *138*, 054117.
(40) Abraham, M. J.; Murtola, T.; Schulz, R.; Páll, S.; Smith, J. C.; Hess, B.; Lindahl, E. GROMACS: High Performance Molecular Simulations through Multi-Level Parallelism from Laptops to Supercomputers. *SoftwareX* **2015**, *1-2*, 19−25.
(41) Hess, B.; Bekker, H.; Berendsen, H. J. C.; Fraaije, J. G. E. M. LINCS: A Linear Constraint Solver for Molecular Simulations. *J. Comput. Chem.* **1997**, *18*, 1463−1472.
(42) Bussi, G.; Donadio, D.; Parrinello, M. Canonical Sampling through Velocity Rescaling. *J. Chem. Phys.* **2007**, *126*, 014101.
(43) Darden, T.; York, D.; Pedersen, L. Particle Mesh Ewald: An N·Log(N) Method for Ewald Sums in Large Systems. *J. Chem. Phys.* **1993**, *98*, 10089−10092.
(44) Yeh, I.-C.; Berkowitz, M. L. Ewald Summation for Systems with Slab Geometry. *J. Chem. Phys.* **1999**, *111*, 3155−3162.
(45) Aksimentiev, A.; Schulten, K. Imaging A-Hemolysin with Molecular Dynamics: Ionic Conductance, Osmotic Permeability, and the Electrostatic Potential Map. *Biophys. J.* **2005**, *88*, 3745−3761.
(46) Zhu, C.; Li, H.; Meng, S. Transport Behavior of Water Molecules through Two-Dimensional Nanopores. *J. Chem. Phys.* **2014**, *141*, 18C528.

DOI: 10.1021/acs.jpcc.7b04283
J. Phys. Chem. C 2017, 121, 13412−13420

(47) Garnier, L.; Szymczyk, A.; Malfreyt, P.; Ghoufi, A. Physics Behind Water Transport through Nanoporous Boron Nitride and Graphene. *J. Phys. Chem. Lett.* **2016**, *7*, 3371−3376.
(48) Luzar, A.; Chandler, D. Effect of Environment on Hydrogen Bond Dynamics in Liquid Water. *Phys. Rev. Lett.* **1996**, *76*, 928.
(49) Corry, B. Mechanisms of Selective Ion Transport and Salt Rejection in Carbon Nanostructures. *MRS Bull.* **2017**, *42*, 306−310.
(50) Israelachvili, J. N. *Intermolecular and Surface Forces*; Academic Press: 2011.

DOI: 10.1021/acs.jpcc.7b04283
J. Phys. Chem. C 2017, 121, 13412−13420